Universiteit Antwerpen

This item is the archived peer-reviewed author-version of:

Accelerated removal of Fe-antisite defects while nanosizing hydrothermal $LiFePO_4$ with Ca^{2+}

Reference:

Paolella Andrea, Turner Stuart, Bertoni Giovanni, Hovington Pierre, Flacau Roxana, Boyer Chad, Feng Zimin, Colombo Massimo, Marras Sergio, Prato Mirko, ...- Accelerated removal of Fe-antisite defects while nanosizing hydrothermal $LiFePO_4$ with Ca^{2+}

Nano letters / American Chemical Society - ISSN 1530-6984 - 16:4(2016), p. 2692-2697

Full text (Publishers DOI): http://dx.doi.org/doi:10.1021/ACS.NANOLETT.6B00334

To cite this reference: http://hdl.handle.net/10067/1336000151162165141

uantwerpen.be

Institutional repository IRUA

NANO LETTERS

Subscriber access provided by UNIV OF CALIFORNIA SAN DIEGO LIBRARIES

Communication

Accelerated Removal of Fe-antisite Defects while Nanosizing Hydrothermal LiFePO4 with Ca2+

Andrea Paolella, Stuart Turner, Giovanni Bertoni, Pierre Hovington, Roxana Flacau, Chad Boyer, Zimin Feng, Massimo Colombo, Sergio Marras, Mirko Prato, Liberato Manna, Abdelbast Guerfi, George P. Demopoulos, Michel Armand, and Karim Zaghib

Nano Lett., **Just Accepted Manuscript** • DOI: 10.1021/acs.nanolett.6b00334 • Publication Date (Web): 11 Mar 2016

Downloaded from http://pubs.acs.org on March 12, 2016

Just Accepted

"Just Accepted" manuscripts have been peer-reviewed and accepted for publication. They are posted online prior to technical editing, formatting for publication and author proofing. The American Chemical Society provides "Just Accepted" as a free service to the research community to expedite the dissemination of scientific material as soon as possible after acceptance. "Just Accepted" manuscripts appear in full in PDF format accompanied by an HTML abstract. "Just Accepted" manuscripts have been fully peer reviewed, but should not be considered the official version of record. They are accessible to all readers and citable by the Digital Object Identifier (DOI®). "Just Accepted" is an optional service offered to authors. Therefore, the "Just Accepted" Web site may not include all articles that will be published in the journal. After a manuscript is technically edited and formatted, it will be removed from the "Just Accepted" Web site and published as an ASAP article. Note that technical editing may introduce minor changes to the manuscript text and/or graphics which could affect content, and all legal disclaimers and ethical guidelines that apply to the journal pertain. ACS cannot be held responsible for errors or consequences arising from the use of information contained in these "Just Accepted" manuscripts.

ACS Publications

Nano Letters is published by the American Chemical Society. 1155 Sixteenth Street N.W., Washington, DC 20036

Published by American Chemical Society. Copyright © American Chemical Society. However, no copyright claim is made to original U.S. Government works, or works produced by employees of any Commonwealth realm Crown government in the course of their duties.

Accelerated Removal of Fe-antisite Defects while Nanosizing Hydrothermal $LiFePO_4$ with Ca^{2+}

Andrea Paolella [a], Stuart Turner [b], Giovanni Bertoni [c], Pierre Hovington [a], Roxana Flacau [d], Chad Boyer [d], Zimin Feng [a], Massimo Colombo [e], Sergio Marras [e], Mirko Prato [e], Liberato Manna [e], Abdelbast Guerfi [a], George P. Demopoulos [f], Michel Armand [g] and Karim Zaghib [a,]*

[a] IREQ - Institute Recherche d`HydroQuebec 1800 Boulevard Lionel Boulet, Varennes, QC J3X 1S1, Canada

[b] EMAT, University of Antwerp, Groenenborgerlaan 171, BE 2020 Antwerp, Belgium

[c] IMEM-CNR, Parco Area delle Scienze 37/A, 43124 Parma, Italy

[d] National Research Council of Canada, Chalk River Laboratories, Chalk River, Ontario K0J 1J0, Canada

[e] Istituto Italiano di Tecnologia, via Morego 30, 16130 Genova, Italy

[f] McGill University, Mining and Materials Engineering Department, Wong Building, 3610 University Street, Montreal QC H3A 0C5, Canada

[g] CICenergigune - Parque Tecnologico C/Albert Einstein 48 CP 01510 Minano (Alava) Spain

***corresponding author**: zaghib.karim@ireq.ca;

Abstract

Based on neutron powder diffraction (NPD) and high angle annular dark field – scanning transmission electron microscopy (HAADF-STEM), we show that calcium ions help eliminate the Fe-antisite defects by controlling the nucleation and evolution of the $LiFePO_4$ particles during their hydrothermal synthesis. This Ca-regulated formation of $LiFePO_4$ particles has an overwhelming impact on the removal of their iron antisite defects during the subsequent carbon-coating step, since: (i) almost all the Fe-antisite defects aggregate at the surface of the $LiFePO_4$ crystal when the crystals are small enough and (ii) the concomitant increase of the surface area, which further exposes the Fe-antisite defects. Our results not only justify a low-cost, efficient and reliable hydrothermal synthesis method for $LiFePO_4$, but also provide a promising alternative viewpoint on the mechanism controlling the nanosizing of $LiFePO_4$, which leads to improved electrochemical performances.

Keywords: antisite, $LiFePO_4$, calcium, surface, defects, hydrothermal

Introduction

Since the early development of $LiFePO_4$[1] great efforts have been dedicated to the study of this material due to its superior safety, high stability and suitable operating voltage (~3.4 V). Olivine $LiFePO_4$ has a *Pnma* structure with lithium ions confined in the channels (M1 site) formed by interconnecting FeO_6 octahedra (M2 site) and PO_4 tetrahedra. Among all the proposed synthesis methods[2-3-4-5], hydrothermal route is likely the cheapest one to prepare $LiFePO_4$. However this method leads to a large fraction of Fe - antisite defects in

the final product and there is to date no procedure that can avoid their formation when using the hydrothermal approach[6-7]. According to current understanding, the Fe-antisite defects can be slowly reduced only by long synthesis time (5-7 hours at 180-200 °C)[8], the use of alcoholic solvent (ethylene glycol or ethanol) instead of water[9-10] or by annealing at high temperature (T > 600 °C)[2]. The important studies of Graetz (via in situ X-ray diffraction)[11-12], Iversen (via neutron powder diffraction)[13] and Ikuhara (via HAADF-STEM)[14] demonstrated that the Fe-antisite defects are formed by Fe-ions located in M1 sites and block the Li^+ diffusion pathway. The Fe-antisite defects are known to be located mainly at the surface of the crystals[15] and can be largely eliminated during the synthesis by a slow cation exchange reaction with a Li-rich amorphous layer that is in close contact with the crystal. In this work we show that calcium ions can facilitate an efficient and complete removal of Fe-antisite defects. This procedure works in two steps: i) by the addition of calcium sulphate to the starting mix we observed the formation of nanocrystals at the early stage of the hydrothermal synthesis of $LiFePO_4$ in contrast to micron size crystals as reported previously[15], ii) since the Fe-antisite defects aggregate at the surface of the crystals, a subsequent carbon coating procedure can completely remove the defects. Regardless of the presence of calcium, the Fe-antisite defects always aggregate mainly at the crystal surface. The effects of calcium ions are on the one hand to regulate nucleation and limit the growth of LFP particles to nanometer scale and on the other hand to promote the aggregation of the Fe-antisite defects at the surface.

Results and discussion

In this work we compared two different hydrothermally synthesized $LiFePO_4$ samples: the classical hydrothermal $LiFePO_4$ (named LFP) and the calcium ion mediated hydrothermal $LiFePO_4$ synthesis (named Ca:LFP). LFP and Ca:LFP were synthesized following the recipe described in the Methods section. We analyzed four different intermediates collected at different times: 10 minutes, 15 minutes, 30 minutes and 5 hours (see Methods section). We investigated the LFP and Ca:LFP samples after 15 minutes of synthesis. The samples were analysed via XRD and HAADF-STEM measurements (see **Figure 1**). The shapes of the crystals synthesized with the two methods are distinctly different. The LFP sample at 15 minutes is in the form of micron sized hexagonal hollow crystal, with a 4 nm thick amorphous layer as previously reported[15]. The Ca:LFP sample instead is in the form of rhombic crystal, with an average amorphous layer of only 1 nm thick (see **Figure S1** in S.I.).

Also, the Ca:LFP sample shows a homogenous distribution of calcium inside the $LiFePO_4$ crystals (see **Figure 2**): the total amount of calcium ions inside $LiFePO_4$ being only around 0.1 - 0.3%, as determined by EDS. These data are consistent with compositional analysis by Time of Flight Secondary Ion Mass Spectroscopy (TOF-SIMS) (see **Figure S4** in S.I). According to the XRD measurements, Li_3PO_4 and β-$Ca_3(PO_4)_2$ were detected as impurities. The observation of calcium phosphate segregation from olivine $LiFePO_4$ is in agreement with paleographic finds[16] and melt casting synthesis[17] while other bivalent ions like Mg^{2+}, Mn^{2+}, Co^{2+}, Ni^{2+} easily form solid solutions[2]. Also, XRD analysis helped to shed light on the formation and growth mechanism of Ca:LFP (see Method section and S.I.): after 10 minutes of synthesis, NH_4LiSO_4, Li_3PO_4 and β-

$Ca_3(PO_4)_2$ phases were detected (see **Figure S2** in S.I.) while only a tiny amount of $LiFePO_4$ was present. Considering i) the formation of Li_3PO_4 and β-$Ca_3(PO_4)_2$ as first intermediate instead of vivianite[15]; ii) the gradual disappearance of Li_3PO_4 and β-$Ca_3(PO_4)_2$ and the formation of $LiFePO_4$; iii) the presence of residual Ca inside the crystal (see **Figure 2** and **Figure S4** in S.I.); iv) the presence of Ca-rich phase around $LiFePO_4$ we suggest that $LiFePO_4$ is formed by gradual reaction of Fe^{2+} with a lithium-calcium based phosphate precursor (e.g $LiCa_{10}(PO_4)_7$ see simulations in S.I.). We believe this proposed reaction pathway can be partially supported by our first principles calculations (see Method section and s.i). With equal amount of atoms, Li_3PO_4 plus $Ca_3(PO_4)_2$ has higher total electronic energy than $LiCaPO_4$. And an exchange of cations Ca^{2+} with Fe^{2+} in dilute aqueous solutions is also energetically favored. And due to the fact that ion-exchanging intercalation reactions happen much more slowly than the other reactions, we explained the existence of $LiCaPO_4$ as an intermediate product.

The Ca:LFP crystals are mainly composed of smaller nanocrystals that are assembled in a rhombic structure as shown in **Figure 3a-b**. Brunauer- Emmett- Teller (BET) analysis (see **Table 1**) highlights a significant increase of the surface area at 15 minutes in the presence of Ca (19 m^2/g for Ca:LFP Vs. 7.3 m^2/g for LFP sample), consistent with a smaller average dimension of the crystals at this stage of the synthesis At 30 minutes the Ca:LFP crystals have a surface area of 9.1 m^2/gr while the LFP crystals only 6.3 m2/g. Finally after 5 hours of synthesis the surface areas become comparable (~5 m^2/gr).

Table 1: *surface area of LFP and Ca:LFP samples by BET analysis.*

Sample	Surface area [m^2/g]			
	15 min	30 min	5h	15 min-Carbon coated
LFP (ref 15)	7.3	6.2	5.4	4.2
Ca:LFP	19.1	9.1	4.6	17.4

According to NPD, the evolution of Fe-antisites during crystal formation was the following (see Methods section and corresponding refinements in S.I.): at 15 minutes the percentage of Fe-antisites exhibited by these two samples was almost the same: 7-8% of Fe atoms in M1. After 30 minutes of synthesis, 4% of Fe atoms were in M1 sites in the LFP[15] sample compared to 1% for the Ca:LFP sample. Only after 5 hours of synthesis, the percentage of Fe-antisites for the two samples was found once again comparable (~1-2%)[15]. HAADF-STEM analysis (**Figure 4)** showed that the standard hydrothermal LFP sample (without calcium) after 15 minutes of synthesis exhibits a higher percentage of Fe-antisites in the bulk compared to the Ca:LFP sample (see **Figure 4a-b**) in which the Fe-antisites were more densely confined at the surface (see **Figure 4c-d**). After 15 minutes of synthesis, the presence of calcium did not alter the percentage of the Fe-antisite defects but promoted the formation of nanoparticles (instead of micron-sized particles) with a higher density of Fe-antisite defects at their surface. As such, the calcium ions favour the formation of high surface $LiFePO_4$ crystals in which the Fe-antisite defects are aggregated on a thin surface layer compared to LFP crystals synthesized without calcium additive (**Figure 4e**). We conclude that during synthesis the formation of nanoparticles by the action of calcium ions accelerates the elimination of Fe-antisites in comparison with the classical LFP synthesis: in the presence of Ca, the percentage of Fe-antisites was reduced from 8% after 15 minutes to ~1-2% at 30 minutes,

with Ca instead of 4% as previously reported for the classical Ca-free $LiFePO_4$ synthesis[15].

After carbon coating of the samples (see Methods section and XRD patterns in **Figure S3** of S.I.) we performed electrochemical tests. After 15 minutes the LFP sample exhibited a capacity of only 40 mAh/g at C/12 and 30 mAh/g at 10 C (see **Figure 5a-b**) while the Ca:LFP had a capacity of 120 mAh/g at C/12 and 70 mAh/g at 10C. The addition of calcium strongly improved the performance at this stage. It must be noted that, in the Ca:LFP sample Li_3PO_4 was still present as impurity (see **Figure S3**).

According to the XRD, the as-synthesized LFP sample collected after 15 minutes was composed of pure $LiFePO_4$ while NPD revealed the presence of 7-8 % of Fe-atoms in M1 sites. The same percentage of Fe-antisite defects was detected on the as-synthesized Ca:LFP sample after 15 minutes. Therefore the two samples have the same amount of defects at the early stages of the synthesis. For LFP (without calcium), the sample after carbon coating was characterized by a reduction in the percentage of the Fe-antisite defects, which dropped from 8 % to 3.5 %. These observations indicate that the antisite defects are not completely eliminated by the annealing treatment, instead a fraction of them is simply relocated out of the crystal forming new impurities ($Fe_2P_2O_7$, see **Figure S11** in S.I.). The percentage of antisite defects in the Ca:LFP sample after the carbon coating step was instead negligible (see S.I. for more details). We also observed the formation of $Fe_2P_2O_7$ in this case while no $Fe_2P_2O_7$ was observed in the LFP@C sample (Fe-antisite defects free) obtained after 5 hours of synthesis. This impurity was already detected after carbon coating by Wang et al.[18] at the surface of $LiFePO_4$ and recently by

Masquelier et al.[19] in deficient Li-ion $LiFePO_4$ structure. These results are in agreement with the observations by HAADF-STEM imaging (**Figure 6**). In the case of LFP, Fe-antisite defects were still observed at the surface of the crystals (see **Figure 6b**) while no Fe-antisite defects at the surface were detected on Ca:LFP crystals (**Figure 6a**). Moreover along the [010] orientation in LFP crystals (without calcium), we observed the epitaxial growth of magnetite Fe_3O_4 nanoparticles (see **Figure S17**). One conclusion that can be drawn from these data is that the initial surface area becomes a key parameter in order to remove Fe-antisites facilitating the intercalation/deintercalation process of lithium ions.

The middle panels of **Figure 5** refer to samples prepared with a 30 minutes synthesis followed by a carbon coating step: the LFP sample evidenced 75 mAh/g capacity at C/12 and only 25 mAh/g capacity at 10C. On the other hand, the Ca:LFP sample exhibited much higher capacities: 140 mh/g at C/ 12 and 75 mAh/g at 10 C. The two pristine samples have a different percentage of Fe-antisite defects and different surface area values: the classical LFP sample had 4% of antisite defects[15] and a surface area of 6.2 m^2/g while Ca:LFP shows ~ 1% of antisite defects (see S.I.) and a surface area of 9.1 m^2/g, thus an increase of ~50%. The removal of Fe-antisites during the synthesis and by carbon coating step is clearly facilitated by nanosizing of LFP. The performances of Ca:LFP after 30 minutes of synthesis were comparable to those of the Ca:LFP sample with 10% of calcium after 5 hours of synthesis (see synthesis in Methods section and **Figures S2** and **S18**) due the presence of residual β-$Ca_3(PO_4)_2$ as impurity.

The 5 hours LFP and Ca:LFP samples had the same percentage of antisite defects, the same surface area and they exhibited comparable electrochemical performances (see **Figure 5**), in agreement with the literature[20-21]. Electrochemical impedance spectra (EIS, in the form of Nyquist plots) of the LFP@C and Ca:LFP@C electrodes at the fully lithiated state ($LiFePO_4$) after 15 minutes, 30 minutes and 5 hours of synthesis are reported in **Figure S19**. In the spectra the intercept on the real axis (Z real) corresponds to the electrolyte resistance (Re), and the semicircle in the middle of the high-frequency region (100 to 1 kHz) is related to the charge transfer resistance (Rct ~50−150 Ω) for the Li transfer across the crystals electrode/electrolyte interface. After 15 minutes LFP@C and Ca:LFP@C exhibited a comparable charge transfer resistance that is probably due to the presence of high amount of lithium at the surface compared to 30 minutes and 5 hours LFP samples[15]. After 30 minutes and 5 hours of synthesis the Ca:LFP@C (blue curves) sample exhibited a charge transfer resistance that was lower than LFP@C (red curves), mainly due to the improvement of electronic conductivity for Ca-sample after Fe-antisites removal. As control experiments, to confirm the unique behaviour of calcium ions in LFP hydrothermal synthesis, we replaced Ca^{2+} with Mg^{2+} (being magnesium a metal alkaline earth as calcium as well) in 15 minutes synthesis (see Methods section for more details). According to XRD measurement (see **Figure S4**) $Li_{0.95}Mg_{0.05}FePO_4$ was detected (with Mg^{2+} ions occupying M1 sites). By EDS and TOF-SIMS we observed a homogenous distribution of Mg^{2+} ions inside the crystals (Mg around 3% vs Fe) meaning a good solubility of magnesium ions inside the olivine structure in agreement with Whittigham`results[2] (see **Figure S5** and **S8**). By XRD and mapping, no Mg-rich phosphate crystals were detected. The surface area of the particles is 3.4 m^2/g (much

lower than Ca:LFP particles at this stage). Then we performed carbon coating and we made electrochemical tests: the performance of the sample is very poor (~40 mAh/g at C/12, see **Figure S20**). These results confirm the unique of calcium ions in hydrothermal $LiFePO_4$ synthesis due to its low solubility in olivine structure.

In conclusion beyond the known benefits of $LiFePO_4$ nanosizing[22], the nucleation path, in this case regulated by the presence of calcium ions, strongly contributes to the removal of Fe-antisite defects at the surface of small LFP crystals. These results are in agreement with recent studies of Tao`s group[23] according to which the Fe-antisite defects tend to aggregate and the denser aggregation is at the surface which helps their elimination. The addition of calcium sulphate as additive could be industrially relevant in order to develop faster and therefore low cost hydrothermal synthesis of $LiFePO_4$ by favoring the effective elimination of antisite defects via segregation in a thinner surface layer.

Materials and methods

Chemicals iron sulphate heptahydrate $FeSO_4 \cdot 7H_20$ (purity ≥ 99.0%), calcium sulphate dihydrate (purity ≥ 99.0%), magnesium sulfate anhydrous $MgSO_4$, lithium hydroxide monohydrate $LiOH \cdot H_20$ (purity ≥ 98.0%), phosphoric acid H_3PO_4 (85% w/w in water, ≥99.9 % trace metals basis), ammonium hydroxide NH_4OH (solution 28.0-30.0% NH_3 basis) and ascorbic acid $C_6H_8O_6$ (purity ≥ 99.0%) were purchased by Sigma Aldrich.

Hydrothermal synthesis of $LiFePO_4$ (LFP) In a standard hydrothermal synthesis 33.6 gr (0.12 mol) of $FeSO_4 \cdot 7H_2O$, 15,41 gr (0.36 mol) of $LiOH \cdot H_2O$, 13,83 gr (0.12 mol) of

H_3PO_4, 0.5 gr of Ascorbic acid ($C_6H_8O_6$) are mixed with 300 ml of deionised water in a glass liner. The final molar ratio between Li: Fe:PO_4:$C_6H_8O_6$ was 3:1:1:0.008. The pH was controlled at 7.8 by drop-wise addition of ammonium hydroxide NH_4OH. The synthesis is performed in a stirred autoclave (OM-JAPAN). We collected intermediates at different times in the heating ramp (from RT to 180 °C in 30 minutes): after 15min (120°C), and after 30min (intermediate at the end of the heating ramp, the temperature was 180 °C). Then the last sample was collected after 5 hours at 180°C.

Hydrothermal synthesis of 3% Ca - $LiFePO_4$ (Ca:LFP) At the synthesis described above is added $CaSO_4 \cdot 2\ H_2O$: 32.68 gr (0.1164 mol) of $FeSO_4 \cdot 7H_2O$ are mixed with 0.62 gr (0.0036 mol) of $CaSO_4 \cdot 2\ H_2O$. The total amount of mol of bivalent cation (Calcium and Iron) is kept fixed to 0.12 mol. The pH was controlled at 7.8 by drop-wise addition of ammonium hydroxide NH_4OH. The synthesis is performed in a stirred autoclave (OM-JAPAN). We collected intermediates at different times in the heating ramp (from RT to 180 °C in 30 minutes): after 10 minutes of synthesis (at the temperature approximately of 90°C), after 15min (120°C), and after 30min (intermediate at the end of the heating ramp, the temperature was 180 °C). Then the last sample was collected after 5 hours at 180°C. About the 5 hours synthesis of Ca:$LiFePO_4$ with 10% of calcium we used 30.02 gr (0.108 mol) of $FeSO_4 \cdot 7H_2O$ and 2.06 gr (0.0036 mol) of $CaSO_4 \cdot 2\ H_2O$.

Hydrothermal synthesis of 3% Mg - $LiFePO_4$ (Mg:LFP) - 15 minutes At the synthesis described above is added $MgSO_4$: 32.68 gr (0.1164 mol) of $FeSO_4 \cdot 7H_2O$ are mixed with 0.72 gr (0.0036 mol) of $MgSO_4$. The total amount of mol of bivalent cation (Magnesium

and Iron) is kept fixed to 0.12 mol. The pH was controlled at 7.8 by drop-wise addition of ammonium hydroxide NH_4OH. The synthesis is performed in a stirred autoclave (OM-JAPAN) for 15 minutes reaching approximatively a temperature of 120 °C.

Carbon coating and electrode preparation For all the samples: 5.66 gr of a lactose aqueous solution (10% w/w) were mixed with 5 gr of $LiFePO_4$ for 30 minutes (5 gr of powder including all the possible impurities). Then the final slurry was annealed in a carbon boat at 95°C overnight and then annealed at 700°C for 3 hours under nitrogen. The $LiFePO_4$ sample carbon coated (89% w/w) was mixed with Denka Carbon (3%), VGCF (3%) and PVDF (5%) and N-methyl pyrrolidone (NMP) as solvent. After mixing with SPEX the final slurry was laminated on aluminium foil. Initially the electrode was dried for 24 h at 75 °C under nitrogen flow just to remove NMP. After lamination and punching, the electrode was dried at 120°C for 5 h under vacuum.

X - Ray Diffraction Analysis XRD patterns were recorded on a Rigaku SmartLab X-Ray diffractometer equipped with a 9kW CuKα rotating anode (operating at 40 kV and 150 mA) and D/teX Ultra 1D detector set in X-ray fluorescence reduction mode. The diffraction patterns were collected at room temperature in Bragg-Brentano geometry over an angular range $2\theta = 15°- 80°$, with a step size of 0.02°. XRD data analysis was carried out using PDXL 2.1 software from Rigaku.

Time of Flight Secondary Ion mass analysis (TOF-SIMS) was performed using a newly develop TOF-SIMS for TofWerk (Germany) mounted on a dual beam (focussed ion

beam and electron beam, Tescan Lyra 3 (Czech Republic)). A Ga+ beam at 30kV was used for the TOF-SIMS measurement and only positive ion was measured.

Brunauer- Emmett- Teller (BET) measurements. Specific surface area measurements were carried out by nitrogen physisorption at 77 K in a Quantachrome equipment, model autosorb iQ. The specific surface areas were calculated using the multi-point BET (Brunauer–Emmett–Teller) model, considering 11 equally spaced points in the P/P_0 range from 0.05 to 0.35. Prior to measurements, samples (50 to 200 mg in form of powder) were degassed for 1 hour at 30°C under vacuum to eliminate weakly adsorbed species.

Transmission Electron Microscopy (TEM). High angle annular dark field images (HAADF) were acquired on a FEI Titan 'cubed' microscope equipped with a CEOS probe corrector. The imaging conditions were: 300 kV electron beam energy and a 21 mrad convergence semi-angle, leading to 0.08nm probe size. The acceptance semi-angle of the annular detector was set to 50-160 mrad.

Neutron powder diffraction (NPD) Powder neutron diffraction (NPD) patterns were collected at C2 High Resolution Powder Diffractometer, NRU reactor, Chalk River Laboratories at room temperature conditions, using vanadium sample cans. The instrument is equipped with a 800-wire position-sensitive detector covering a range of 80 degrees. 1.328 Å wavelength neutrons were used to measure the data in 2θ range of 5 to 117 degrees, with a step size of 0.1 degrees. The data were analysed using FullProf Suite[24]. We performed the refinements using the following constrain[13]: i) fully

occupancy of Fe in M2 sites and ii) lithium occupancy was calculated by occ (Li) = 1 - 2*occ (Fe). No extra Li-vacancies were considered[15].

Electrochemical measurements: The 2032 coin-type cells (20-mm diameter and 3.2-mm thick) were assembled in a glove box in a high purity argon atmosphere. The cell consisted of the cathode, Li metal anode, microporous membrane (Celgard 2400) separator and a non-aqueous electrolyte of 1M $LiPF_6$ in ethylene carbonate (EC): dimethyl carbonate (DMC) (1:1v/v). The cells were cycled at 25 °C between 2.0 and 4.0 V vs. Li^0/Li^+ at constant current on a battery cycler. About the calculation of the capacity, we considered 89% of active material as composed by pure $LiFePO_4$, and then some capacity underestimation was possible.

Calculation method: our density functional theory calculation is performed using the VASP package[25] with the Project augmented wavefunction framework[26-27] and Perdew-Burke-Enzerhof exchange-correlation functional[28]. A Hubbard U correction with a value of 3.7eV is added to the d-electrons on Fe atoms, as suggested by Zhou et al.[29]. All structures are relaxed until the maximum forces on the atoms are less than 0.01eV/Å. The solvation free energies of Ca^{2+} and Fe^{2+} are adopted from Markus[30].

Acknowledgments

The authors want to acknowledge Prof. J.B Goodenough of Texas University, Vincent Gariepy, Daniel Clement, Julie Trottier and Catherine Gagnon of IREQ, Dr.Chandramohan George of Cambridge University, Dr. Maria Filipousi of EMAT for helpful discussions. Z.F. would like to express his great thankfulness to Dr. Qi Shuai for

the enlightening discussions. S.T. gratefully acknowledges the fund for scientific research Flanders (FWO) for a post-doctoral scholarship.

Authors information

Corresponding author:

*Email: zaghib.karim@ireq.ca

Notes

The authors declare no competing financial interest.

Supporting Information

HR(S)TEM and EDS images, XRD patterns, TOF-SIMS analysis, Neutron powder diffraction pattern refinements and electrochemical measurements are included in Supporting Information. This material is available free of charge at http://pubs.acs.org.

References

(1) Padhi, A. K., Nanjundaswamy, K. S. and Goodenough, J. B. J. Electrochem. Soc. 1997, 144, 1188-1194.

(2) Yang, S., Song, Y., Zavalij, P. Y. and Whittingham, M. S. Electrochem. commun. 2002, 4**,** 239–244.

(3) Wang, L., He, X., Sun, W., Wang, J., Li, Y., Fan, S. Nano Lett. , 2012, 12, 5632–5636.

(4) Hsu, K., Tsay, S. and Hwang, B. J. Mater. Chem. 2004, 14, 2690–2695

(5) Park, K S., Kang, K. T., Lee, S. B., Kim, G. Y., Park, Y. J., Kim, H. G., Mater. Res. Bull. 2004, 39, 1803–1810.

(6) Wang, J. & Sun, X. Energy Environ. Sci. 2012, 5, 5163–5185

(7) Wang, J. & Sun, X. Energy Environ. Sci. 2015, 8, 1110–1138.

(8) Chen, J. & Whittingham, M. S. Electrochem. commun. 2006, 8, 855–858.

(9) Qin, X., Wang, J., Xie, J., Li, F.,Wang, X., Phys. Chem. Chem. Phys. 2012, 14, 2669-2677

(10) Cho, M. Y., Kim, K. B., Lee, J. W. Kim, H., Kim, H., Kang, K., Chul Roh, K., RSC Adv. 2013, 3, 3421

(11) Chen, J., Bai, J., Chen, H. & Graetz, J. J. Phys. Chem. Lett, 2011.. 2**,** 1874–1878

(12) Chen, J. & Graetz, J. ACS Appl. Mater. Interfaces 2011, 3**,** 1380–1384

(13) Jensen, K. M. Ø., Christensen, M., Gunnlaugsson, H. P., Lock, N., Bøjesen, E. D., Pro, T., Iversen, B. B., Chem. Mater. 2013, 25, 2282–2290

(14) Chung, S.-Y., Choi, S.-Y., Yamamoto, T. & Ikuhara, Y. Angew. Chem. Int. Ed. Engl. 2009, 48, 543–546.

(15) Paolella, A., Bertoni, G., Hovington, P., Feng, Z., Flacau, R., Prato, M., Colombo, M., Marras, S., Manna, L., Turner, S., et al. Nano Energy , 2015, 16, 256–267.

(16) Fransolet, M. Bull. Soc. Fr. Miner. Cristal. 1972, 100, 198–207

(17) Gauthier, M., Michot, C., Ravet, N., Duchesneau, M., Dufour, J., Liang, G., Wontcheu, J., Gauthier, L., Macneil, D D, J. Electrochem. Soc. 2010, 157, A453–A462

(18) Wang, J., Yang, J., Tang, Y., Liu, J., Zhang, Y., Liang, G., Gauthier, M., Chen-wiegart, Y. K., Banis, M. N., Li, X. et al. Nat. Commun. 2014, 5, 1–8

(19) Amisse, R., Sougrati, M. T., Stievano, L., Davoisne, C., Draz, G., Budic, B., Dominko, R., Masquelier, C., Chem. Mater. 2015, 27, 4261–4273

(20) Dokko, K., Koizumi, S., Sharaishi, K. & Kanamura, K. J. Power Sources 2007, 165, 656–659

(21) Murugan, A. V., Muraliganth, T. & Manthiram, A. J. Phys. Chem. C 2008, 112**,** 14665–14671

(22) Lee, K. T., Kan, W. H. & Nazar, L. F.. J. Am. Chem. Soc. 2009, 131, 6044–6045

(23) Boyang, H. & Guohua, T. J. Mater. Chemsitry A 2015, 3, 20399-20407

(24) Rodriguez-carvajal, J. neutron powder diffraction. Phys. B. 1993, 192, 55–69

(25) Kresse, G. & Furthmuller, J. Phys. Rev. B. 1996, 54, 11169–11186

(26) P E, B. Phys. Rev. B. 1994, 50, 17953–17979

(27) Kresse, G. & Joubert, D. Phys. Rev. B. 1999, 59, 1758–1775

(28) Perdew, J. P., Burke, K. & Ernzerhof, M. Phys. Rev. Lett. 1996, 3865–3868

(29) Wang, L., Zhou, F., Meng, Y. S. & Ceder, G. Phys. Rev. B. 2007, 76, 165435

(30) Marcus, Y. J. Chem. Soc. Faraday Trans. 1991, 87, 2995–2999

Figures

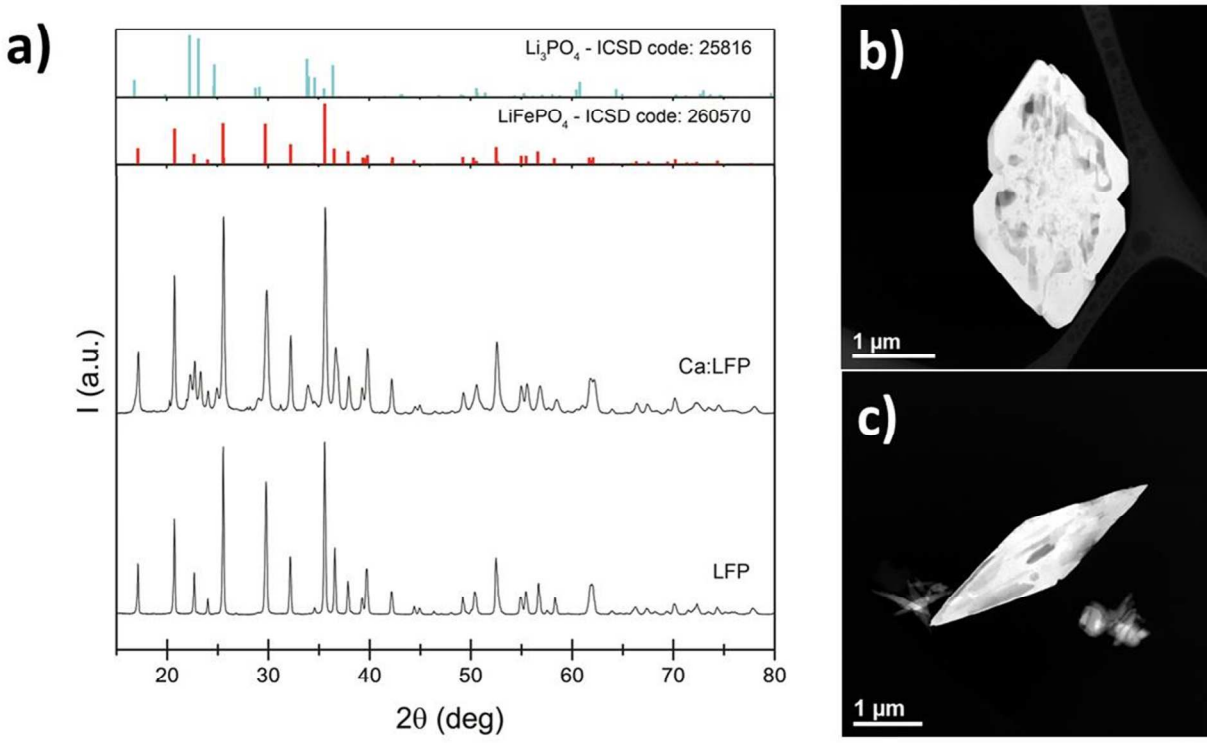

Figure 1: *a) XRD patterns, b) STEM image of standard hydrothermal LFP and c) STEM image of calcium modified hydrothermal LFP*

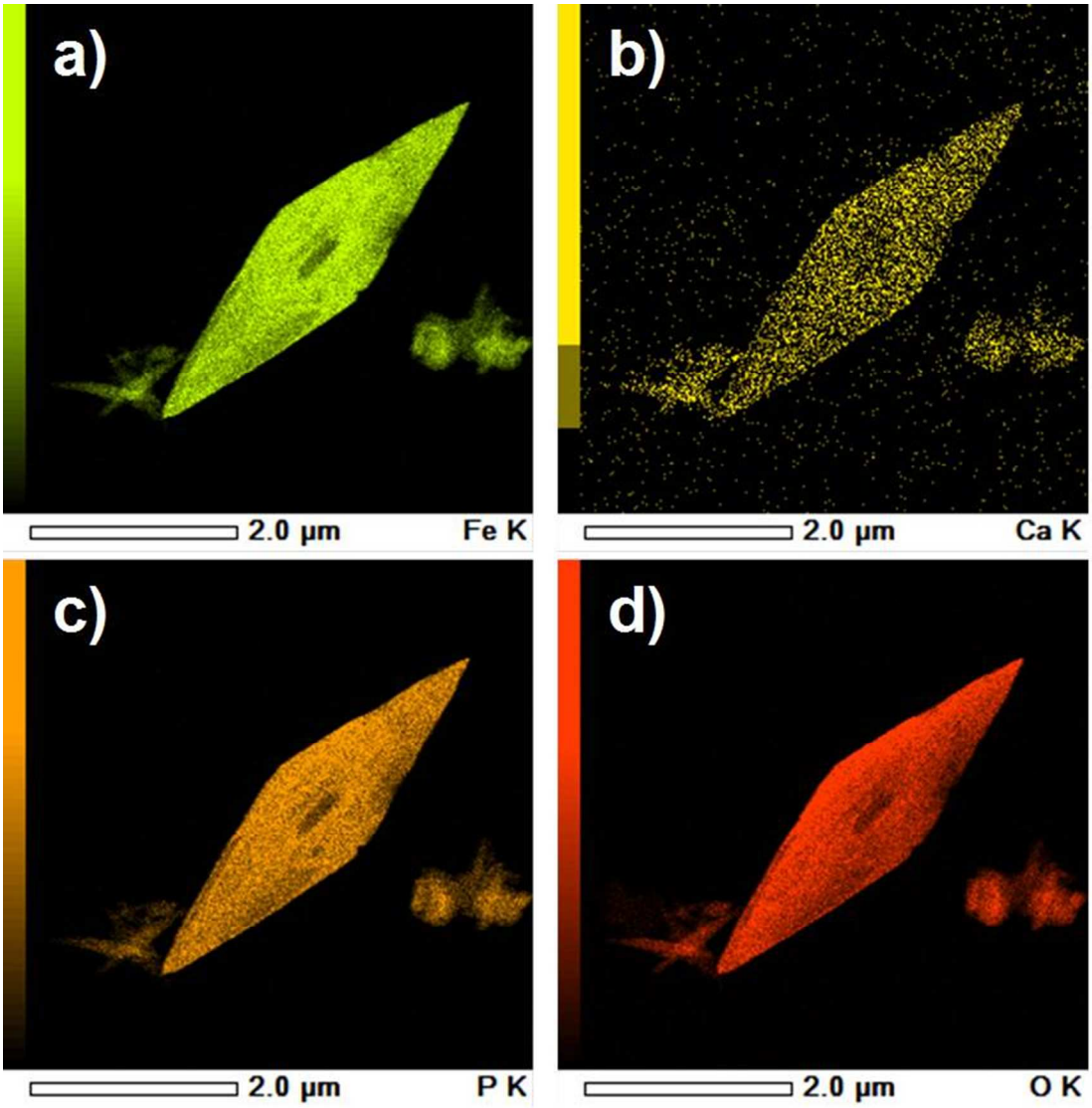

Figure 2: *EDS image mapping on hydrothermal Ca:LFP sample showing the homogenous distribution of a) iron, b) calcium, c) phosphorus and d) oxygen ions inside Ca: LiFePO4 crystals*

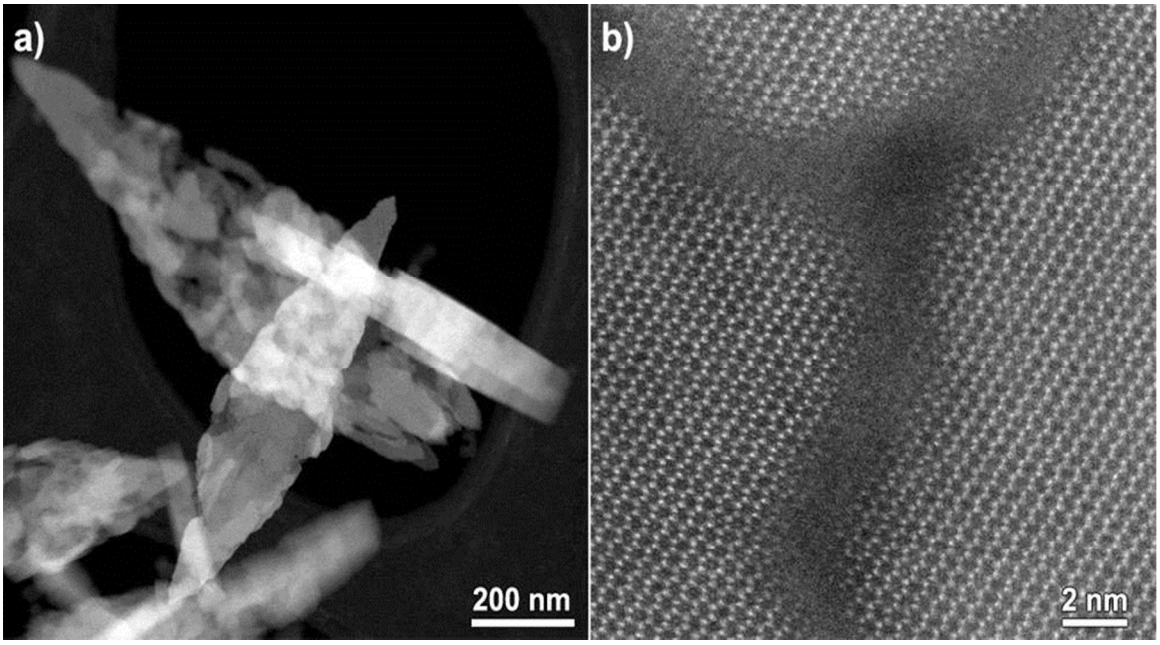

Figure 3: *a) HAADF-STEM image of the porous $LiFePO_4$ crystals and b) high resolution HAADF-STEM image of amorphous regions within individual crystals (synthesis made using 3% of calcium ions and 15 minutes of synthesis).*

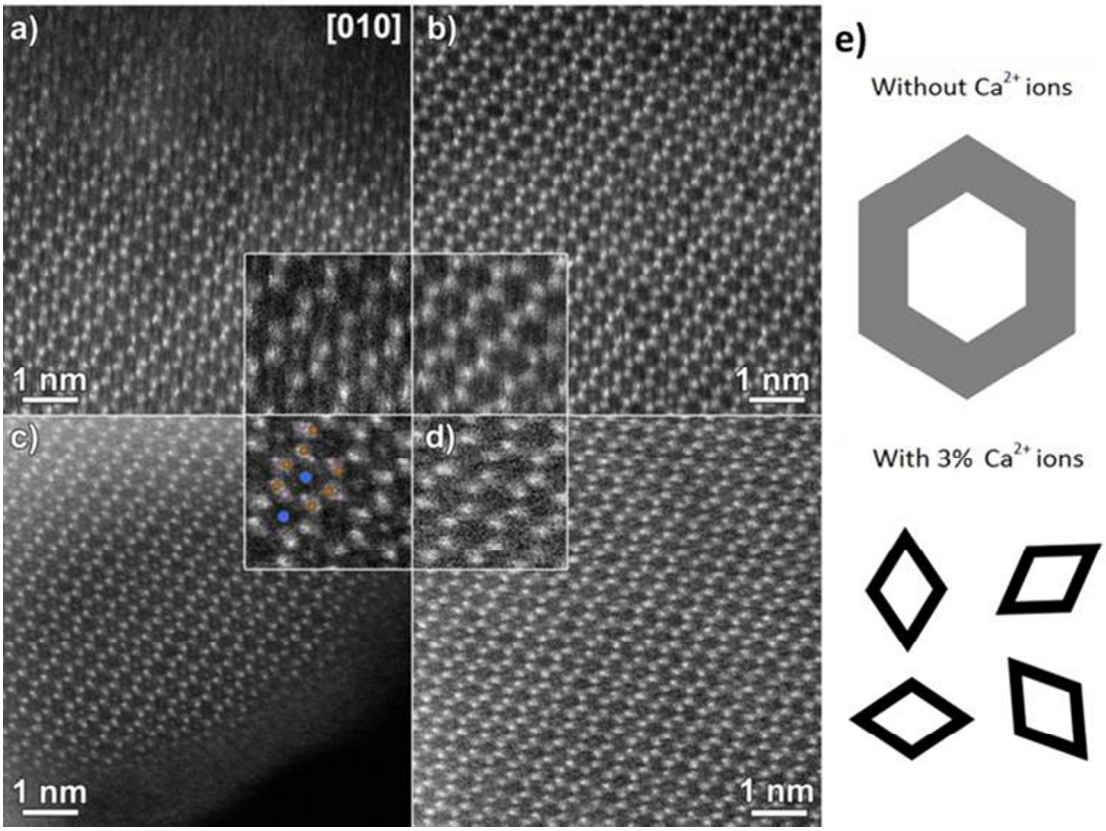

Figure 4: *High resolution HAADF-STEM images of Fe-antisite defects in a) surface and b) bulk of LFP; c) surface and d) bulk of Ca:LFP. Inset: enlarged regions of a)-d) with an overlaid structural model with Fe in brown, P in purple and the Li antisite position in blue (oxygen positions are not shown for clarity) in c). e) antisite distribution models for LFP and Ca:LFP.*

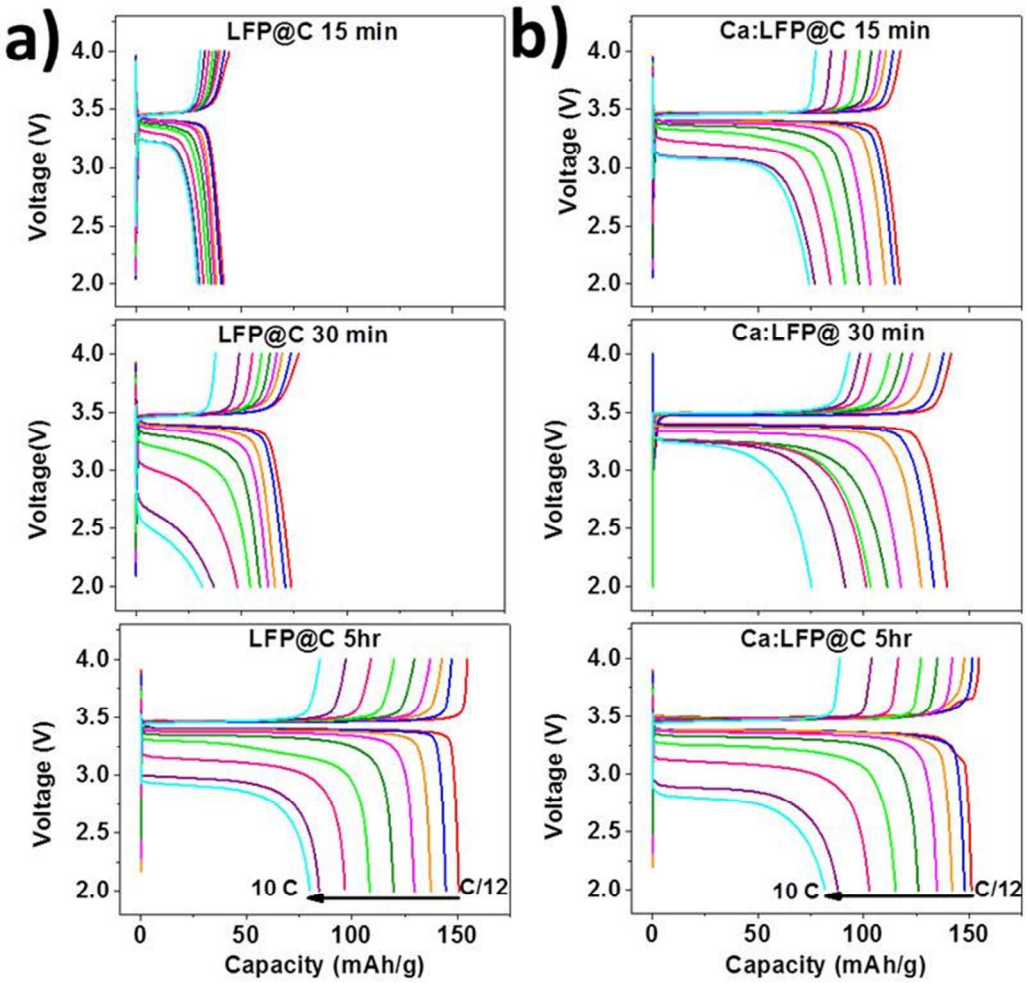

Figure 5: *charge/discharge curves at different C rate for $LiFePO_4$ without calcium a) and b) $LiFePO_4$ with 3% of calcium after 15 minutes,30minutes and 5 hours of synthesis. The discharge rate C/12 is in red, C/8 in blue, C/4 in orange, C/2 in magenta, 1C in olive green, 2C in green, 4C in pink, 8C in purple and 10C in cyan.*

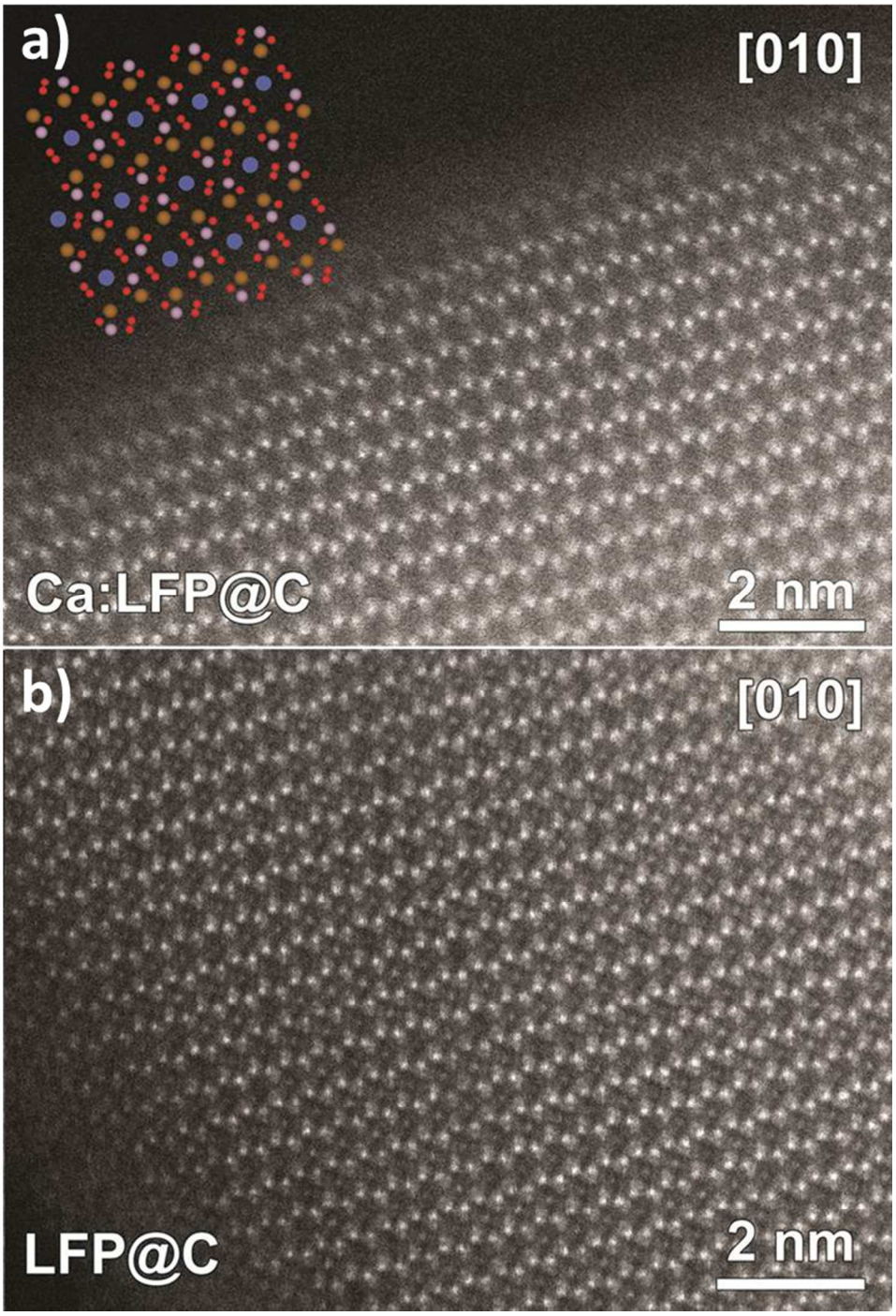

Figure 6: *a) HAADF-STEM image of 3% Ca-LFP@C showing an absence of Fe-antisites at the surface with an overlaid structural model with Fe in brown, P in purple, the Li antisite position in blue and oxygen positions in red. b) HAADF-STEM image of LFP@C showing the presence of Fe-antisites at the surface.*

TOC Graphic